Journal of Applied Physics ARTICLE scitation.org/journal/jap

Direct detection of rare earth ion distributions in gallium nitride and its influence on growth morphology

Cite as: J. Appl. Phys. **127**, 013102 (2020); doi: 10.1063/1.5134050
Submitted: 30 October 2019 · Accepted: 20 December 2019 ·
Published Online: 3 January 2020

B. Mitchell,[1,2,a)] D. Timmerman,[2] W. Zhu,[2] J. Y. Lin,[3] H. X. Jiang,[3] J. Poplawsky,[4] R. Ishii,[5] Y. Kawakami,[5] V. Dierolf,[6] J. Tatebayashi,[2] S. Ichikawa,[2] and Y. Fujiwara[2]

AFFILIATIONS

[1]Department of Physics, West Chester University, West Chester, Pennsylvania 19383, USA
[2]Division of Materials and Manufacturing Science, Graduate School of Engineering, Osaka University, 2-1 Yamadaoka, Suita, Osaka 565-0871, Japan
[3]Department of Electrical and Computer Engineering, Texas Tech University, Lubbock, Texas 79409, USA
[4]Center for Nanomaterials Science, Oak Ridge National Laboratory, Oak Ridge, Tennessee 37830, USA
[5]Department of Electronic Science and Engineering, Kyoto University, Kyoto 615-8510, Japan
[6]Department of Physics, Lehigh University, Bethlehem, Pennsylvania 18015, USA

Note: This paper is part of the Special Topic on Defects in Semiconductors 2020.
[a)]**Author to whom correspondence should be addressed:** bmitchell@wcupa.edu

ABSTRACT

The dopant distribution and surface and structural properties of Er- and Eu-doped GaN samples were investigated using atom probe tomography (APT) and atomic force microscopy (AFM). Erbium accumulation within host GaN threading dislocations was directly detected by APT allowing for the dislocations to be imaged in three dimensions. In addition, photoluminescence spectroscopy with high lateral resolution, by means of scanning near-field optical microscopy, was performed on Eu-doped GaN samples. By combining these results with AFM mappings of the same area, it was concluded that Eu^{3+} ions also accumulate at threading dislocations. Moreover, high-resolution surface profiles of both samples show that even dilute doping (<0.2%) of Eu and Er has a significant influence on the growth morphology of the GaN host material and the nature of the threading dislocations within it. Transmission electron microscopy techniques were used to show the influence of rare-earth incorporation on the growth of GaN lattice and the propagation of threading dislocations.

I. INTRODUCTION

Gallium nitride has had an extraordinary impact on the optoelectronics industry with a wide range of applications in photonics, green and blue light-emitting diodes (LEDs), and high-power blue lasers.[1–7] Despite the overwhelming attention that this system has received, several issues still remain, such as the high threading dislocation density (TDD) of GaN grown by metal-organic chemical vapor deposition (MOCVD) on c-plane sapphire substrates ($\sim 10^8$–10^{10} cm^{-2}) and the development of a practical GaN-based red LED, for example, using InGaN quantum wells.[8,9] Threading dislocations (TDs) arise because of the lattice mismatch between the sapphire substrate and the GaN and can act as nonradiative recombination centers in GaN-based LEDs.[4,10–12] In addition, the strain induced from the lattice mismatch also enhances the piezoelectric polarization fields that occur within the InGaN quantum wells, which results in lower radiative recombination rates of electrons and holes due to the quantum-confined Stark effect.[8,9,13,14]

TDD has been directly linked to the lifetime and efficiency of GaN-based laser diodes, which has been attributed to their impact on the threshold current of the devices.[3,4,15] For heteroepitaxially grown GaN layers, three types of threading dislocations (TDs) occur, which are known as edge, screw, and mixed type, because the line direction often runs parallel with the [0001] direction.[16] Screw- and mixed-type

are known to be easily observed for relatively large-scale atomic force microscopy (AFM) due to their large cores.[17,18] To reduce the TDD, several techniques have been established such as epitaxial layer overgrowth (ELOG),[19–21] selective area growth (SAG),[22–24] and the use of patterned sapphire substrates.[25] For ELOG and SAG, the TDD was reduced only from 10^8–10^9 to 10^6–10^7 cm^{-2}, and the growth was changed from the usual step-flow to three-dimensional growth in order to relax the lattice. An alternate method is to use bulk GaN substrates with the TDDs of $\sim 10^5$–10^6 cm^{-2}, which can be grown by hydride vapor-phase epitaxy (HVPE).[26]

Rare-earth (RE) doped wide-gap semiconductors are of great interest for applications in light-emitting diodes, because of their sharp and stable emission, temperature stability, and the possibility of current injection.[27,28] As mentioned above, while blue and green LEDs have already been successfully commercialized, efficient red emission from GaN remains a challenge due to the quantum-confined Stark effect, among other practical complications such as the immiscibility of In.[4,8,12] Eu-doped GaN attracts much attention for its intense red emission originating from the intra-4*f* shell transitions of trivalent Eu^{3+} ions, where the emission intensity from GaN:Eu-based LEDs has exceeded 1 mW.[29–41] Trivalent erbium (Er^{3+}) has received attention due to the transition from its first excited state $^4I_{13/2}$ to the ground state $^4I_{15/2}$, which results in emission at 1.54 μm. Er-doped GaN has potential applications as an emitter or optical waveguide amplifier at the optical communication wavelength.[42–45] In addition, room temperature light amplification has been achieved from GaN:Er quantum well structures.[46] Given the prevalence of TDs in GaN, it is important to understand the interaction of RE ions with TDs, and the impact that this interaction has on the growth morphology of the host crystal.

In this contribution, a systematic study of Eu- and Er-doped GaN samples was performed. Multiple microscopy and spectroscopy techniques were employed to investigate the effect of *in situ* RE doping on the structural properties of the MOCVD-grown GaN, and its influence on the optical properties of the RE ions. The results show that the RE ions interact with charged defects such as threading dislocations. This interaction can be modified by changing the substrate, sample structure, and growth temperature, which has a significant influence on the growth morphology of the GaN host and the optical properties of the RE ions.

II. MATERIALS AND METHODS

A. Sample growth

Several GaN:Eu samples grown by organometallic vapor-phase epitaxy (OMVPE) were used in this study, one sample was grown on a c-plane HVPE-GaN substrate, while all other samples were grown on (0001) sapphire substrates. All samples were initiated with a 30 nm low temperature (900 °C) GaN buffer layer, followed by a 2 μm thick undoped GaN layer grown at 1200 °C. The gallium and nitrogen sources were TMGa and ammonia and the reactor pressure was 100 kPa. The Eu-precursor used in this system was $EuCp_2^{pm}$.[41] The primary difference between samples was the growth temperature, sample thickness, and sample structure of the Eu-doped layer deposited on top of the 2 μm undoped GaN layer.

Two samples had a 300 nm layer of GaN:Eu grown at 1030 °C, where Ar diluted O_2 was supplied at a flow rate of 200 slm during growth. One sample was grown on an HVPE-GaN substrate and the other was grown on a sapphire substrate. Additional oxygen is needed to stabilize the Eu incorporation in these two samples, since $EuCp_2^{pm}$ was used as the Eu source and the growth temperature was above 1000 °C.[38,39] Also, 200 slm was found to be the optimal flow rate at 1030 °C.[38] Another sample consisted of a 300 nm layer of GaN:Eu grown at 960 °C, as this was found to improve the Eu incorporation and emission intensity without the external addition of oxygen.[39] For two other samples, a multilayer structure (MLS) was used as it was shown to be beneficial for the luminescence properties and dopant location in the GaN host for low-oxygen-containing samples.[36,38] The MLS samples consisted of 40 pairs of 10 nm thick GaN layers and 3 nm thick GaN:Eu layers. One MLS sample was grown at 1030 °C, which we'll call the higher temperature MLS (HT-MLS) and one MLS was grown at 960 °C, which we'll call the lower temperature MLS (LT-MLS).[38,40] Two devices were also made using the 10:3 GaN/GaN:Eu layer ratio MLS as the active layer, and details on the device structure can be found elsewhere.[39,40] In order to ensure that measurements of AFM and scanning near-field optical microscopy (SNOM) assess the same area on a sample, a metal marker with a thickness of 50 nm was introduced with a $\sim$8 μm width, which was formed by photolithography and the liftoff technique.[17]

Three Er-doped samples grown by MOCVD were used in this study, where the PL characteristics and crystalline quality were previously measured.[42–45] No additional oxygen was needed for the Er incorporation in these samples, due to the oxygen present in the Er precursor. Two of the samples were started by depositing a $\sim$1.2 μm GaN layer on either a (0001) sapphire or an HVPE c-plane GaN substrate, which was then followed by a GaN:Er epilayer with a thickness of 1 μm. The gallium and nitrogen precursors were also TMGa and ammonia, and tris(2,2,6,6-tetramethyl-3,5-heptanedionato) erbium was the metal-organic precursor used for the *in situ* Er doping. The growth temperature was 1040 °C for all samples, and the Er concentration was $\sim 6 \times 10^{19}$ cm^{-3}.[45–47] Eu and Er concentrations of $\sim 5 \times 10^{19}$ cm^{-3} were close to the resolution limit of atom probe tomography (APT). Therefore, to detect an accumulation of Er atoms, another GaN:Er sample with a concentration of $\sim 5 \times 10^{20}$ cm^{-3} was used.[43,44]

B. Atom probe tomography and atomic force microscopy

Atomic force microscopy (AFM) was used to investigate the surface morphologies of the samples (Hitachi-AFM5100N). Certain features of the surface were more easily observed in one mode or another. For measurements that focused on shallower surface features such as hill-locks, force maps were used to display the surface profile of the GaN and GaN:Eu, as these features were found to be more easily observed in this mode. When the deeper surface pits that were found on the surface of MOCVD-grown GaN were the feature of focus, contact mode AFM images were presented, although it should be noted that the shallower surface features could still be observed, just not as clearly as in the force mode. For all GaN:Er samples, both surface features and pits could be observed in the contact mode, and therefore, the contact mode was used to display all AFM scans for GaN:Er.

Atom probe tomography (APT) was performed to investigate the doping profile of the samples. A standard wedge lift-out technique was used for APT sample preparation using a Thermo Fisher Nova 200 dual beam focus ion beam (FIB)/scanning electron microscope (SEM), in which wedge pieces were mounted on a Si microtip array and annular milled into needle-shaped specimens. A 30 kV accelerating voltage was used for annular milling followed by a 2 kV cleaning step to remove the Pt cap and Ga ion-induced surface damage, and to obtain a resulting initial needle radius of approximately 50 nm.[48] The GaN needles were run in a CAMECA LEAP 4000X-HR with a 50 kHz pulse frequency, 2% detection rate, ~0.2 pJ laser energy resulting in a Ga+/Ga++ peak ratio of ~50, and a base temperature of 25 K. The low pulse rate was used to limit the effects of DC heating, which results in a larger signal-to-noise ratio than higher pulse rates. A slightly higher than normal laser power was also used to increase the signal-to-noise ratio such that the dopant distribution could be detected.

C. Scanning near-field optical microscopy

SNOM-PL measurements were performed in illumination-collection mode, where photoexcitation and PL collection is performed in the same probe,[49] at room temperature using a fiber probe with an aperture diameter of 220 nm. A continuous wave InGaN laser diode emitting at 405 nm was used for sub-bandgap excitation of the Eu^{3+} ions, while a He-Cd laser operating at 325 nm was used for above bandgap excitation. The spatial resolution for these parameters is in the order of 100 nm. Photoluminescence signals were collected by a monochromator with a liquid-nitrogen-cooled charge-coupled-device (CCD) detector; therefore, the system could acquire the PL spectrum at each measurement point.

D. Transmission and scanning transmission electron microscopy

To investigate the influence of RE ion doping on the crystallinity of the GaN layers, cross-sectional TEM and STEM samples were prepared from an LT-MLS LED wafer. First, the samples were cleaved to remove the sapphire substrate and mechanically polished to a thickness of ~10 μm. Next, the samples were further thinned down to less than 100 nm using an Ar ion beam in a Gatan Precision Ion Polishing System (PIPS) (model 691). In this paper, bright-field TEM images were acquired using a Hitachi H-800. For atomic level resolution images, high-angle annular dark-field scanning transmission electron microscopy (HADDF-STEM) with Corrector-Spherical Aberration system (JEOL ARM-200F) was chosen. Since HADDF has more sensitivity to RE and gallium than other light elements (such as nitrogen), it was possible to discern the disordering of gallium atoms by RE ion doping at the atomic level.

III. RESULTS

A. Substrate dependence on surface morphology

Figure 1 shows the AFM force map surface profiles of GaN and RE-doped GaN samples grown on sapphire and GaN substrates. The surface of a standard GaN sample is shown in Fig. 1(a),

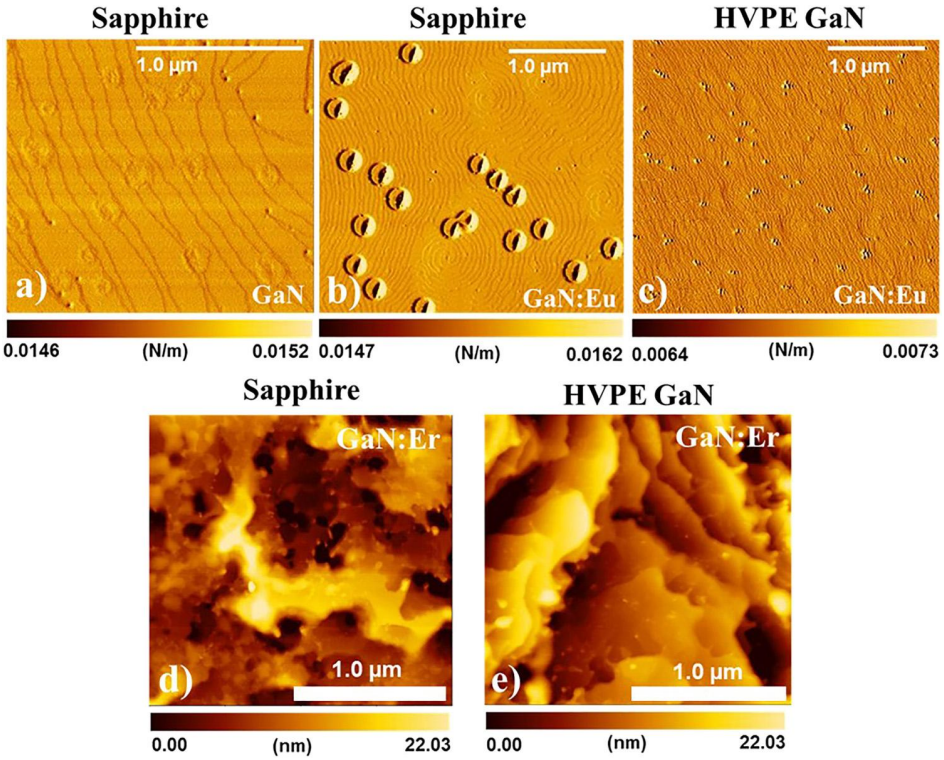

FIG. 1. AFM surface profiles of (a) 2.0 μm of GaN grown on sapphire. (b) 300 nm of Eu-doped GaN grown on top of 2.0 μm of GaN on sapphire. (c) 300 nm of Eu-doped GaN grown on top of 2.0 μm of GaN on HVPE-GaN. (d) 1.0 μm of Er-doped GaN grown on top of 1.2 μm of GaN on sapphire. (e) 1.0 μm of Er-doped GaN grown on top of 1.2 μm of GaN on HVPE-GaN. Force maps are used for (a)–(c), and standard AFM profiles are used for (d) and (e).

and relatively uniformly grown steps can be observed. Surface pits are present at the location of open-core TDs, and the density of these pits is $\sim 3 \times 10^8$ cm^{-2}, which is a typical value found in GaN grown on sapphire via MOCVD.[18–23,26] When Eu is doped into GaN on a sapphire substrate at 1030 °C, the surface morphology changes substantially, as seen in Fig. 1(b). The diameter of the surface pits increases to ~100 nm and several spiral structures or "hill-locks" can be observed.[18] This is similar to InGaN with high In concentrations.[50–52] The hill-locks are most likely caused by the larger size of the Eu ions compared to Ga, which disrupts the growth. Several of the TDs have a screwlike character, and the growth layer is displaced when it encounters a Eu^{3+} ion, which can result in the formation of a large hill in the AFM scan with a screw-like character.[50,53] When the Eu is doped into GaN grown on a GaN substrate under the same growth conditions, the hill-locks and large pits are not observed [Fig. 1(c)]. Similarly, spiral features and large pits are also observed on the surface of Er-doped GaN grown on sapphire, but not on samples grown on GaN [Figs. 1(d) and 1(e)]. It should be noted that the concentration of Eu and Er is similar in all samples, although the surface roughness of the Er samples is considerably greater, yet key characteristics of growth on HVPE-GaN vs sapphire are still shared. Since HVPE-GaN substrates contain far less threading dislocations ($\sim 10^5$–10^6 cm^{-2}), it is inferred that the formation of hill-locks and enlargement of the surface pits is due to an interaction of the RE atoms with the TDs that form between the GaN buffer layer and the sapphire substrates.

B. Er distribution revealed through atom probe tomography

To explore the interaction of the RE atoms with TDs, atom probe tomography was performed on an Er-doped GaN sample grown on sapphire with an Er concentration of $\sim 5 \times 10^{20}$ cm^{-3}. The APT reconstruction shown in 90-degree rotational views is shown in Figs. 2(a) and 2(b) with the 3D distribution of Er atoms shown as green points and a 0.3 at. % Er isoconcentration surface encapsulating a region that has >0.3 at. % Er contents. The rotations show that the Er decorates a linear feature that is diagonally intersecting the APT needle and is not associated with a pole. Figure 2(c) displays a 1D concentration profile across the Er enriched feature, which shows that the Er concentration is as much as 5× greater inside the isosurface than in the matrix. From the diameter and shape of the isosurface, it is concluded that the isosurface most likely represents Er accumulation near a TD.

C. Spatially resolved photoluminescence

Unfortunately, Eu accumulation at a dislocation was not directly observed in GaN:Eu, but the volume of the sample analyzed by APT is very small. Therefore, there could be Eu clustering in these samples despite the absence of clustering in the APT data. To evaluate a larger sample volume with high spatial resolution, PL measurements were performed using an SNOM to investigate the Eu distribution near TDs. First, room temperature PL spectra were taken on the HT-MLS sample in the far-field for two different excitation wavelengths, 325 nm for above bandgap excitation and 405 nm for below bandgap excitation. The PL spectra are depicted in Fig. 3, and it can be observed that for excitation above bandgap, the spectrum is broader and contains more features as compared to the spectrum obtained under below bandgap excitation. For the GaN:Eu system, it is known that the Eu incorporates into different defect environments or "centers," where two of these centers, commonly labeled as OMVPE4 and OMVPE7,[30–39] are the most influential in terms of the optical properties of the material. OMVPE4

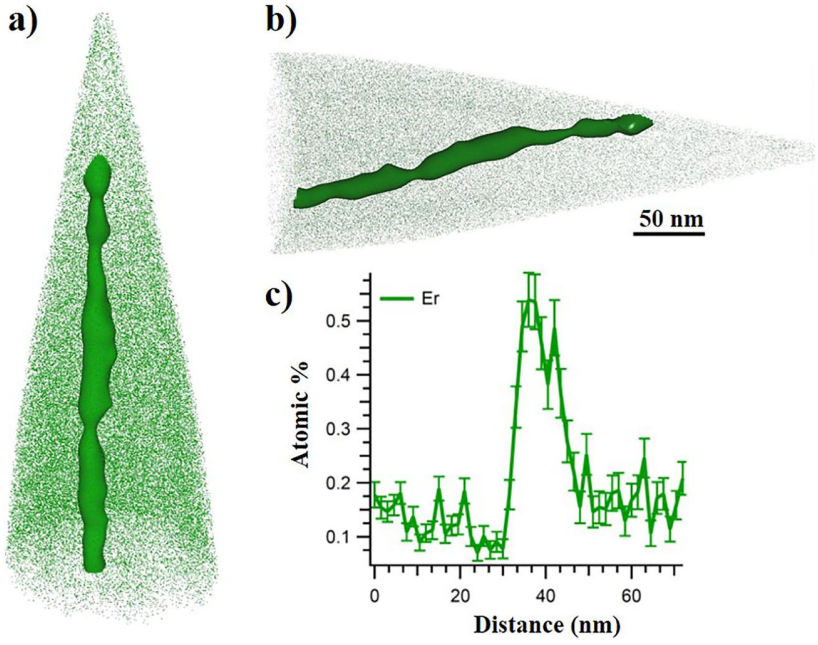

FIG. 2. (a) A reconstructed APT image of an Er doped GaN sample showing the Er atoms as green dots and a 0.3 at. % isoconcentration surface. (b) A 90-degree rotated view of the APT image in (a), which shows that the isoconcentration surface moves diagonally through the APT dataset. The size and the shape of this region indicate that the Er is accumulating around a GaN threading dislocation. (c) A 1D concentration profile across the Er enriched region. Multimedia views: https://doi.org/10.1063/1.5134050.1; https://doi.org/10.1063/1.5134050.2

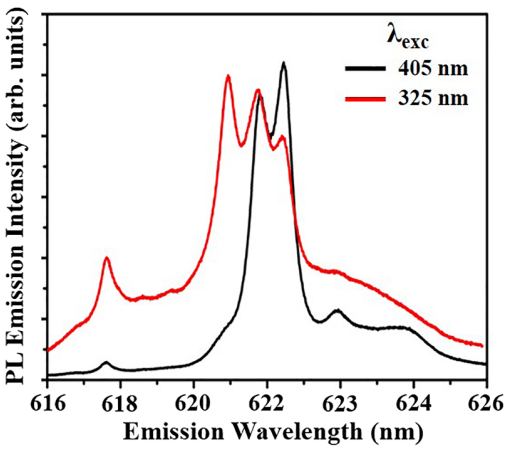

FIG. 3. Far-field PL spectra of the HT-MLS sample under optical excitation below (405 nm) and above (325 nm) the GaN bandgap energy.

is the majority center in GaN:Eu, comprising over 75% of the Eu incorporation, while PL emission from OMVPE7 is the most prominent for above bandgap excitation, despite its much lower abundance (≈4%).[30–39]

In Fig. 4(a), an image of the metal marker with a square hole as taken with an optical microscope is shown on the left. The square center is approximately $8 \times 8\,\mu$m, and defines the area that is studied by AFM and SNOM. The AFM image on the right side of Fig. 4(a) depicts the high-resolution topography of the center square and the surrounding metal marker. Threading dislocations, which show up as ∼100 nm large pits, can be clearly observed on this scale, and are indicated by the white circles. From the AFM image, the TD dislocation density is determined to be $\sim 2.6 \times 10^8\,\mathrm{cm}^{-2}$ for the combined screw and mixed type. The PL intensity of the area was mapped by selectively exciting the OMVPE4 center under 405 nm excitation, and the resulting PL intensity is shown in Fig. 4(b). In this map, the collected spectra at each collection point were fitted with the Eu emission spectrum in order to get the PL intensity related to the Eu^{3+} ions. A strongly nonhomogenous intensity distribution is observed, with areas of strong and weak emission intensity from OMVPE4. In the same figure, the location of the threading dislocations is depicted as determined from the AFM mapping. The PL data were overlaid with 100 nm diameter spots at the locations of the TDs in Fig. 4(b), and the average PL intensity within the 100 nm spot was calculated. This was repeated for spot diameters of 200 nm and 400 nm centered on the TDs and compared with the average intensity of the whole area within the square, which is shown in Fig. 4(c). It is clear that the average PL intensity is significantly higher closer to the

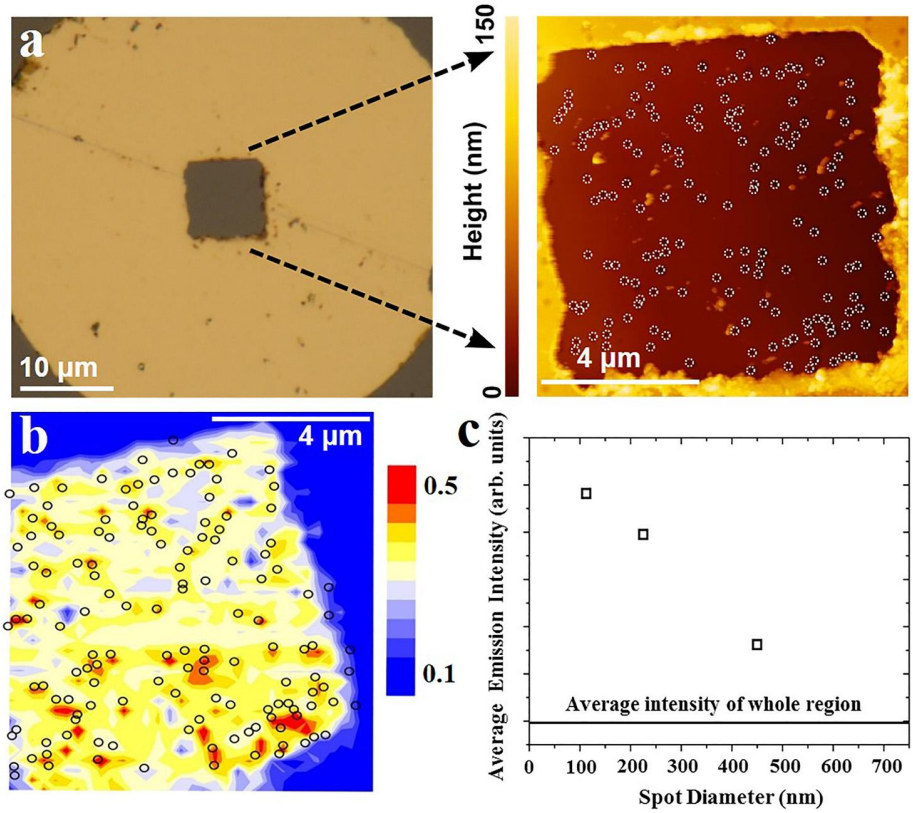

FIG. 4. (a) Left: Optical image of the metal marker deposited on the sample surface. Right: AFM scan of the area defined by the metal marker. The white circles indicate threading dislocation positions. (b) PL intensity mapping of the Eu-related emission. Black circles indicate the threading dislocation positions as determined from the AFM mapping. (c) The PL data were overlaid with 100 nm, 200 nm, and 400 nm diameter spots at the location of the TDs shown in Fig. 4(b). The average PL intensity within spots was calculated and compared against the average intensity of the whole area within the square.

dislocations. This indicates that there is an accumulation of OMVPE4 centers near TDs. Higher Er contents were also found near TDs by APT. It may also be possible that increased light extraction close to the TDs could play a role in this observation; however, there are some regions near TDs with significantly lower emission than in the bulk.

D. Growth temperature and sample structure dependence on surface morphology

The growth temperature was found to have a significant influence on the emission intensity and defect profile of Eu-doped layers and devices grown using $EuCp_2^{pm}$ as the Eu precursor. Devices fabricated with the MLS grown at 960 °C exhibited an output power of ~1.25 mW at 20 mA,[36] which is more than an order of magnitude higher than that from the HT-MLS grown at 1030 °C. As the electrical properties of GaN-based devices are partially dependent on the prevalence of TDs and the surface morphology, the surfaces of a variety of GaN:Eu samples grown with different growth temperatures and structures were investigated by AFM. In Figs. 5(a) and 5(b), the surface of a high-quality undoped GaN sample grown on sapphire and a 300 nm bulk Eu-doped sample grown at 1030 °C, are shown for reference. The surface of the HT-MLS structure is shown in Fig. 5(c), and is similar to the surface of the 300 nm continuously grown GaN:Eu sample grown at 1030 °C, which is consistent with the surface profile shown in Fig. 4.

The surface of a sample where the growth temperature of the 300 nm Eu-doped layer is reduced to 960 °C is shown in Fig. 5(d). The diameter of the TD pits is reduced compared to those seen on the surface of the undoped GaN sample on sapphire. Figure 5(e) shows the surface of a 10:3 LT-MLS sample, and no visible pits are observed within the 1 μm × 1 μm AFM scan. Thus, it appears that the lower growth temperature changes the interaction of the Eu atoms with the TDs, which is more pronounced in the LT-MLS sample.

E. Origin of the pit diameter reduction revealed by electron microscopy

To gain more insight into the absence of surface pits for the MLS sample grown at 960 °C, cross-sectional TEM and STEM experiments were performed. Figure 6(a) shows a bright-field cross-sectional TEM image of the 10:3 LT-MLS device with 40 pairs of alternating GaN:Eu/GaN layers. Several TDs can be observed, which originate in the buffer layer and travel to the Eu-doped layer. However, all of the dislocations are bent away from the viewing plane within a few hundred nanometers of entering the LT-MLS region. Figure 6(b) shows a zoomed-in TEM image of the LT-MLS region, and the Eu-doped layers can be seen clearly within the contrast of the image, despite the dilute Eu doping. The contrast most likely originates from strain. It should be noted that the contrast between layers is not observed in HT-MLS structures. It was reported that the Eu atoms form larger and more complex defect

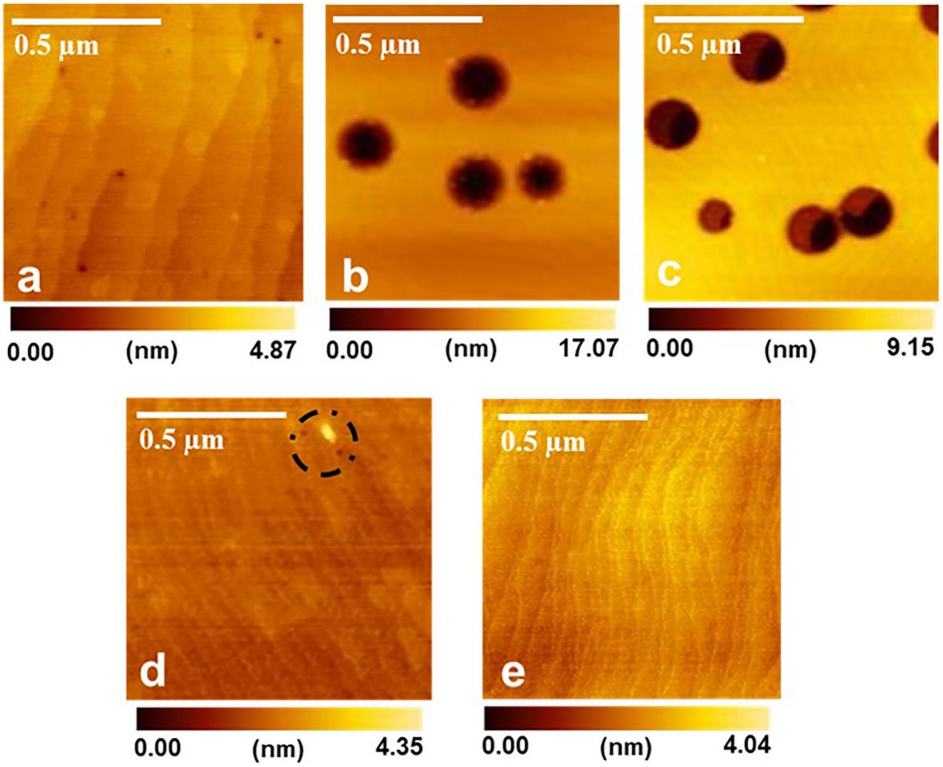

FIG. 5. 1 μm × 1 μm AFM scans of the surfaces of (a) undoped GaN, (b) 300 nm thick GaN:Eu, (c) 10:3 MLS sample grown at 1030 °C, (d) 300 nm bulk GaN:Eu grown at 960 °C, and (e) 10:3 MLS sample grown at 960 °C (LT-MLS). Large pits form when Eu is doped into GaN at 1030 °C. The diameter of the pits at the surface is reduced for growth at 960 °C, and no visible pits are observed on the LT-MLS in the 1 μm × 1 μm region.

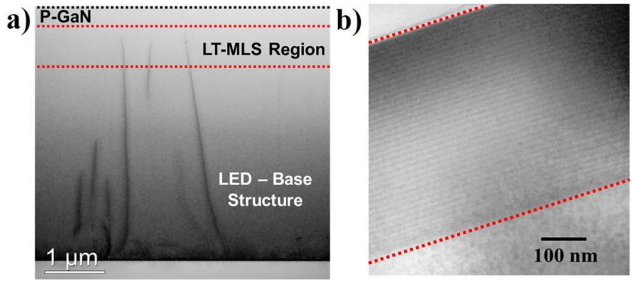

FIG. 6. (a) Cross-sectional TEM image of an LED with the 10:3 LT-MLS as the active layer. The diagram on the right shows the sample structure. Three TDs penetrate into the MLS region; however, they disappear within the layer and do not reach the surface consistent with the AFM results shown in Fig. 5(d). (b) A higher magnification image of the LT-MLS region of the sample shown in (a).

clusters when grown at low temperatures. We believe that lattice distortion caused by these defect clusters results in the higher strain observed in the Eu-doped layers grown at lower temperatures.

Atomic resolution HADDF imaging was performed on the LT-MLS layers to investigate the lattice structure between layers. HADDF images of undoped GaN and of the LT-MLS are shown in Figs. 7(a) and 7(b), respectively. When the two HADDF images are overlapped, the GaN layers in the LT-MLS have the same lattice structure, whereas the lattice is significantly shifted in the 3 nm Eu-doped layer. This shifting of the lattice (i.e., strain) between the Eu-doped and undoped layers is believed to be the cause of the significant bending of the TDs in the LT-MLS samples. It should also be noted that there is one less plane of atoms in the Eu:GaN layer (15 planes) compared to the GaN layer (16 planes).

IV. DISCUSSION

From the AFM images, it is clear that the doping of Eu or Er into GaN grown at high temperatures (>1000 °C) has a detrimental impact on the surface morphology, but only for samples grown on sapphire. The APT results show direct evidence for Er^{3+} ions decoration at TDs. Although Eu accumulation was not observed by APT, the SNOM-PL measurements indicate potential segregation of Eu atoms in the OMVPE4 defect environment toward TDs as inferred from the inhomogeneity of the PL mapping with high-intensity regions being located in the vicinity of TDs. It should be noted that the excitation of the Eu atoms in the SNOM measurements is done below bandgap by a defect-assisted process, which removes an interpretation related to possible preferential diffusing pathways, as observed in the recombination dynamics of nitrides.[54]

Once the growth temperature is reduced below 1000 °C, the luminescence becomes broader, the luminescence intensity of the Eu-doped active layers increases,[36,39,40] and the surface of the samples contains fewer and smaller TD related pits. The defect profile was reported to change significantly in Eu-doped samples grown below 1000 °C. In particular, it was found that V_{Ga}-O complexes are the primary defect in samples grown below 1000 °C, and V_{Ga} sites are the prominent defect in samples grown at higher temperatures.[39] In addition, emission from devices based on the multilayer structure growth at 960 °C becomes broader and more intense, with no clear preference toward OMVPE7.[36,40] The surface of these samples contains almost no visible pits, and electron microscopy confirms that the TDs are significantly perturbed when they enter the LT-MLS region.

Due to the large number of TDs that result from the lack of a lattice matched substrate for GaN growth, several studies have been performed on the interaction of common defects and these dislocations. Dislocations in n-type GaN were found to exist in a negatively charged state as determined by electron holography.[55] Multiple studies have reported that oxygen related defects, which tend to exist in the positive charge state, will segregate toward dislocations, both open- and closed-core.[56–60] The oxygen is attracted to the sides of the dislocations, and is found to decorate their surfaces in GaN.[58,59] This oxygen segregation toward the dislocation can have a substantial impact on the formation dynamics of the dislocations during growth at temperatures above 1000 °C.[59,60] Theoretical studies have shown that the closed-core dislocation, in which the dislocation "collapses," is the equilibrium state of a threading dislocation. Oxygen that has segregated toward a dislocation has a high affinity for 3- "acceptor" defects and will form strong bonds with these defects. The most common 3- defect in n-type GaN is the gallium vacancy (V_{Ga}). In general, dislocations can perpetuate in the open-core state well into the GaN epilayer, and do not simply terminate near the sapphire surface.[58] The V_{Ga}-O complexes are found to stabilize the surface of the dislocation and slow the growth of open-core dislocations.

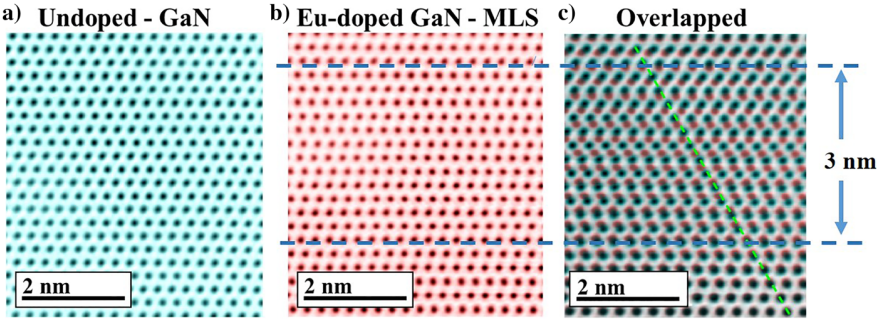

FIG. 7. Atomic resolution HADDF images of (a) undoped GaN and (b) Eu-doped GaN in the LT-MLS, which are overlapped in (c). The lattice is shifted significantly within the 3 nm Eu-doped layer but returns to that of undoped GaN at the barriers. The diagonal dotted line shows that the atomic spacing of the undoped GaN does not change, while the atomic spacing (red dots) of Eu-doped GaN does.

At a critical V_{Ga}-O concentration, no further perpetuation of the dislocation occurs; however, a new edge or threading dislocation can begin to grow.[57–59]

Rare-earth ions exist primarily in the trivalent state (3+) when doped into GaN, which may explain their affinity to segregate toward negatively charged dislocations. The defect center OMVPE4 has been associated with a nitrogen vacancy, whereas OMVPE7 has been associated with a deep acceptor such as a V_{Ga}.[35,39,61] This difference in the defect environment could influence the preferential segregation of certain centers, namely, OMVPE4, toward TDs. In the Eu-doped samples grown at low temperatures, the higher concentration of V_{Ga}-O complexes and significant lattice shift in the Eu-GaN layers grown at 960 °C are believed to be responsible for the bending and narrowing of TDs that enter the LT-MLS region. Moreover, the formation dynamics of TDs change at different temperatures. All of these conditions could account for the surface pit reduction, and more studies are needed to confirm the exact nature behind this phenomenon.

The presented results suggest that the larger luminescence intensity for the LT-MLS sample is due to the reduction of surface pits and TDs, which increases the number of optically active Eu ions under current injection.[36,39,40] It may be that the decorated TDs act as sources of leakage current, as observed for Mg decorated TDs in GaN, and energy is not effectively transferred to Eu atoms in these regions.[62] Additionally, the altering strain barriers between the GaN and GaN:Eu layers could produce a carrier confinement-type effect, which could enhance the carrier capture dynamics in the Eu-doped layers. This is further supported by the observation that the index of refraction of RE-doped GaN is different than that of GaN.[63] Overall, while it is clear that the doping of RE atoms into GaN has an influence on the growth morphology due to accumulation at TDs and strain, further studies are needed to elucidate the mechanisms behind the increase in the luminescence efficiency and reduction of pit density observed for Eu-doped GaN samples grown at lower temperatures.

ACKNOWLEDGMENTS

The MOCVD growth effort is supported by the Army Research Office (ARO) (Grant No. W911NF-09-1-0275) and U.S. Army CERDEC (Grant No. W15P7T-07-D-P040). H.X.J. would like to acknowledge the support of Whitacre endowed chairs through the AT&T Foundation. This work was partly supported by a Grant-in-Aid for Scientific Research (S) (No. JP24226009) from the Japan Society for the Promotion of Science and the Murata Science Foundation, as well as another Grant-in-Aid for Specially Promoted Research (JP18H05212) from the Japan Society for the Promotion of Science. APT was conducted at ORNL's Center for Nanophase Materials Sciences (CNMS), which is a U.S. DOE Office of Science User Facility.

This manuscript has been authored by UT-Battelle, LLC, under Contract No. DE-AC05-00OR22725 with the U.S. Department of Energy. The United States Government retains and the publisher, by accepting the article for publication, acknowledges that the United States Government retains a non-exclusive, paid-up, irrevocable, world-wide license to publish or reproduce the published form of this manuscript, or allow others to do so, for United States Government purposes. The Department of Energy will provide public access to these results of federally sponsored research in accordance with the DOE Public Access Plan (http://energy.gov/downloads/doe-public-access-plan).

REFERENCES

[1]S. Nakamura, T. Mukai, and M. Senoh, Appl. Phys. Lett. **64**, 1687–1689 (1994).
[2]S. Nakamura, M. Senoh, N. Iwasa, S. Nagahama, T. Yamada, and T. Mukai, Jpn. J. Appl. Phys. **34**, L1332–L1335 (1995).
[3]S. Nakamura, M. Senoh, S. Nagahama, N. Iwasa, T. Yamada, T. Matsushita, Y. Sugimoto, and H. Kiyoku, Appl. Phys. Lett. **70**, 1417–1419 (1997).
[4]S. Nakamura, Science **281**, 956–961 (1998).
[5]S. J. Pearton and F. Ren, Adv. Mater. **12**, 1571–1580 (2000).
[6]S. Pimputkar, J. S. Speck, S. P. DenBaars, and S. Nakamura, Nat. Photonics **3**, 180–182 (2009).
[7]A. Gautam and F. C. J. M. vanVeggel, Chem. Mater. **23**, 4817–4823 (2011).
[8]J.-I. Hwang, R. Hashimoto, S. Saito, and S. Nunoue, Appl. Phys. Express **7**, 071003 (2014).
[9]S. Saito, R. Hashimoto, J. Hwang, and S. Nunoue, Appl. Phys. Express **6**, 111004 (2013).
[10]Y. Jiang, Y. Li, Y. Li, Z. Deng, T. Lu, Z. Ma, P. Zuo, L. Dai, L. Wang, H. Jia, W. Wang, J. Zhou, W. Liu, and H. Chen, Sci. Rep. **5**, 10883 (2015).
[11]S. Dang, C. Li, M. Lu, H. Guo, and Z. He, Optik **155**, 26 (2018).
[12]R. Singh, D. Doppalapudi, T. D. Moustakas, and L. T. Romano, Appl. Phys. Lett. **70**, 1089 (1997).
[13]T. J. Baker, B. A. Haskell, F. Wu, J. S. Speck, and S. Nakamura, Jpn. J. Appl. Phys. **45**, L154 (2006).
[14]H. Zhao, G. Liu, X.-H. Li, G. S. Huang, J. D. Poplawsky, S. T. Penn, V. Dierolf, and N. Tansu, Appl. Phys. Lett. **95**, 061104 (2009).
[15]S. Nagahama, N. Iwasa, M. Senoh, T. Matsushita, Y. Sugimoto, H. Kiyoku, T. Kozaki, M. Sano, H. Matsumura, H. Umemoto, K. Chocho, and T. Mukai, Jpn. J. Appl. Phys. **39**, L647–L650 (2000).
[16]M. A. Moram, C. S. Ghedia, D. V. S. Rao, J. S. Barnard, Y. Zhang, M. J. Kappers, and C. J. Humphreys, J. Appl. Phys. **106**, 073513 (2009).
[17]A. Kaneta, M. Funato, and Y. Kawakami, Phys. Rev. B **78**, 125317 (2008).
[18]Z. Chen, L. W. Su, J. Y. Shi, X. L. Wang, C. L. Tang, and P. Gao, "AFM application in III-nitride materials and devices," in *Atomic Force Microscopy—Imaging, Measuring and Manipulating Surfaces at the Atomic Scale*, edited by V. Bellitto (InTech, 2012).
[19]S. Tanaka, M. Takeuchi, and Y. Aoyagi, Jpn. J. Appl. Phys. **39**, L831–L834 (2000).
[20]T. Wang, Y. Morishima, N. Naoi, and S. Sakai, J. Cryst. Growth **213**, 188–192 (2000).
[21]K. J. Lee, E. H. Shin, and K. Y. Lim, Appl. Phys. Lett. **85**, 1502–1504 (2004).
[22]T. S. Zheleva, N. Ok-Hyun, M. D. Bremser, and R. F. Davis, Appl. Phys. Lett. **71**, 2472–2474 (1997).
[23]N. Ok-Hyun, M. D. Bremser, T. S. Zheleva, and R. F. Davis, Appl. Phys. Lett. **71**, 2638–2640 (1997).
[24]H. Marchand, X. H. Wu, J. P. Ibbetson, P. T. Fini, P. Kozodoy, S. Keller, J. S. Speck, S. P. DenBaars, and U. K. Mishra, Appl. Phys. Lett. **73**, 747–749 (1998).
[25]W. Cao, J. M. Biser, Y.-K. Ee, X.-H. Li, N. Tansu, H. M. Chan, and R. P. Vinci, J. Appl. Phys. **110**, 053505-1–053505-4 (2011).
[26]Y. Golan, X. H. Wu, J. S. Speck, R. P. Vaudo, and V. M. Phanse, Appl. Phys. Lett. **73**, 3090–3092 (1998).
[27]A. J. Steckl, J. C. Heikenfeld, M. J. Garter, C. C. Baker, and R. Jones, IEEE J. Sel. Top. Quantum Electron. **8**, 749 (2002).
[28]A. J. Steckl, J. H. Park, and J. M. Zavada, Mater. Today **10**, 20 (2007).
[29]A. Nishikawa, T. Kawasaki, N. Furukawa, Y. Terai, and Y. Fujiwara, Appl. Phys. Express **2**, 071004 (2009).
[30]Z. Fleischman, C. Munasinghe, A. J. Steckl, A. Wakahara, J. Zavada, and V. Dierolf, Appl. Phys. B **97**, 607 (2009).

[31]K. P. O'Donnell, I. S. Roqan, K. Wang, K. Lorenz, E. Alves, and M. Boćkowski, Opt. Mater. **33**, 1063 (2011).
[32]N. Woodward, A. Nishikawa, Y. Fujiwara, and V. Dierolf, Opt. Mater. **33**, 1050 (2011).
[33]K. Lorenz, E. Alves, I. S. Roqan, K. P. O'Donnell, A. Nishikawa, Y. Fujiwara, and M. Boćkowski, Appl. Phys. Lett. **97**, 111911 (2010).
[34]R. Wakamatsu, D. Timmerman, D. Lee, A. Koizumi, and Y. Fujiwara, J. Appl. Phys. **116**, 043515 (2014).
[35]B. Mitchell, J. Poplawsky, D. Lee, A. Koizumi, Y. Fujiwara, and V. Dierolf, J. Appl. Phys. **115**, 204501 (2014).
[36]B. Mitchell, T. Gregorkiewicz, V. Dierolf, and Y. Fujiwara, J. Appl. Phys. **123**, 160901 (2018).
[37]W. Zhu, R. Wei, D. Timmerman, T. Gregorkiewicz, B. Mitchell, Y. Fujiwara, and V. Dierolf, ACS Photonics **5**, 875 (2018).
[38]B. Mitchell, D. Timmerman, J. Poplawsky, W. Zhu, D. Lee, R. Wakamatsu, J. Takatsu, M. Matsuda, W. Guo, K. Lorenz, E. Alves, A. Koizumi, V. Dierolf, and Y. Fujiwara, Sci. Rep. **6**, 18808 (2016).
[39]W. Zhu, B. Mitchell, D. Timmerman, A. Uedono, A. Koizumi, and Y. Fujiwara, APL Mat. **4**, 056103 (2016).
[40]W. Zhu, B. Mitchell, D. Timmerman, A. Koizumi, T. Gregorkiewicz, and Y. Fujiwara, MRS Adv. **2**, 159–164 (2017).
[41]B. Mitchell, A. Koizumi, R. Wakamatsu, D. Lee, Y. Saitoh, D. Timmerman, Y. Kuboshima, T. Mogi, S. Higashi, K. Kikukawa, H. Ofuchi, T. Honma, and Y. Fujiwara, Mater. Chem. Phys. **193**, 140 (2017).
[42]C. Ugolini, N. Nepal, J. Y. Lin, H. X. Jiang, and J. M. Zavada, Appl. Phys. Lett. **90**, 051110 (2007).
[43]R. Dahal, C. Ugolini, J. Y. Lin, H. X. Jiang, and J. M. Zavada, Appl. Phys. Lett. **93**, 033502 (2008).
[44]R. Dahal, C. Ugolini, J. Y. Lin, H. X. Jiang, and J. M. Zavada, Appl. Phys. Lett. **95**, 111109 (2009).
[45]I. W. Feng, J. Li, A. Sedhain, J. Y. Lin, and H. X. Jiang, J. Appl. Phys. Lett. **96**, 031908 (2010).
[46]V. X. Ho, T. M. Al tahtamouni, H. X. Jiang, J. Y. Lin, J. M. Zavada, and N. Q. Vinh, ACS Photonics **5**, 1303 (2018).
[47]N. T. Woodward, N. Nepal, B. Mitchell, I. W. Feng, J. Li, H. X. Jiang, J. Y. Lin, J. M. Zavada, and V. Dierolf, Appl. Phys. Lett. **99**, 122506 (2011).
[48]K. Thompson, D. Lawrence, D. J. Larson, J. D. Olson, T. F. Kelly, and B. Gorman, Ultramicroscopy **107**, 131–139 (2007).
[49]T. Saiki, K. Nishi, and M. Ohtsu, Jpn. J. Appl. Phys. **37**, 1638 (1998).
[50]Z. Liliental-Weber, Y. Chen, S. Ruvimov, W. Swider, and J. Washburn, Phys. Rev. Lett. **79**, 2835–2838 (1997).
[51]Y. Chen, T. Takeuchi, H. Amano, I. Akasaki, N. Yamada, Y. Kaneko, and S. Y. Wang, Appl. Phys. Lett. **72**, 710–712 (1998).
[52]H. K. Cho, J. Y. Lee, G. M. Yang, and C. S. Kim, Appl. Phys. Lett. **79**, 215–217 (2001).
[53]B. Heying, E. J. Tarsa, C. R. Elsass, P. Fini, S. P. DenBaars, and J. S. Speck, J. Appl. Phys. **85**, 6470–6476 (1999).
[54]A. Kaneta, T. Hashimoto, K. Nishimura, M. Funato, and Y. Kawakami, Appl. Phys. Express **3**, 102102 (2010).
[55]D. Cherns and C. G. Jiao, Phys. Rev. Lett. **87**, 205504 (2001).
[56]J. Elsner, R. Jones, M. I. Heggie, P. K. Sitch, M. Haugk, T. Frauenheim, S. Öberg, and P. R. Briddon, Phys. Rev. B **58**, 12571 (1998).
[57]R. Jones, J. Elsner, M. Haugk, R. Gutierrez, T. Frauenheim, M. I. Heggie, S. Öberg, and P. R. Briddon, Phys. Status Solidi A **171**, 167 (1999).
[58]I. Arslan and N. D. Browning, Phys. Rev. Lett. **91**, 165501 (2003).
[59]M. E. Hawkridge and D. Cherns, Appl. Phys. Lett. **87**, 221903 (2005).
[60]E. Baghani and S. K. O'Leary, J. Appl. Phys. **110**, 033509 (2011).
[61]B. Mitchell, N. Hernandez, D. Lee, A. Koizumi, Y. Fujiwara, and V. Dierolf, Phys. Rev. B **96**, 064308-1–064308-8 (2017).
[62]S. Usami, N. Mayama, K. Toda, A. Tanaka, M. Deki, S. Nitta, Y. Honda, and H. Amano, Appl. Phys. Lett. **114**, 232105 (2019).
[63]S. Alajlouni, Z. Y. Sun, J. Li, J. M. Zavada, J. Y. Lin, and H. X. Jiang, Appl. Phys. Lett. **105**, 081104 (2014).